Received: 16 December 2020 | Revised: 19 March 2021 | Accepted: 20 April 2021

DOI: 10.1002/jcc.26553

FULL PAPER

Journal of COMPUTATIONAL CHEMISTRY WILEY

Describing ground and excited state potential energy surfaces for molecular photoswitches using coupled cluster models

Anders Hutcheson[1] | Alexander Christian Paul[1] | Rolf H. Myhre[1] | Henrik Koch[2] | Ida-Marie Høyvik[1]

[1]Department of Chemistry, The Norwegian University of Science and Technology, Trondheim, Norway

[2]Scuola Normale Superiore, Pisa, Italy

Correspondence
Ida-Marie Høyvik, Department of Chemistry, The Norwegian University of Science and Technology, Høgskoleringen 5, 7491 Trondheim, Norway.
Email: ida-marie.hoyvik@ntnu.no

Funding information
Marie Sklodowska-Curie European Training Network, Grant/Award Number: 765739; Norges Forskningsråd, Grant/Award Numbers: 263110, 275506

Abstract

In this article, we use two extensively studied systems, a retinal model system and azobenzene, to explore the use of coupled cluster models for describing ground and singlet excited state potential energy surfaces of photoswitchable systems. While not being suitable for describing nuclear dynamics of photoisomerization, coupled cluster models have useful attributes, such as the inclusion of dynamical correlation, their black box nature, and the systematic improvement offered by truncation level. Results for the studied systems show that when triple excitations (here through the CC3 model) are included, ground and excited state potential energy surfaces for isomerization paths may reliably be generated, also for states of doubly excited character. For ground state equilibrium cis- and trans-azobenzene, the molecular geometry and basis set is seen to significantly impact the vertical excitation energies for the two lowest excited states. Efficient implementations of coupled cluster models can therefore constitute valuable tools for investigating photoswitchable systems and can be used for preliminary black box studies to gather information before more complicated excited state dynamics approaches are pursued.

KEYWORDS
azobenzene, coupled cluster, excited states, penta-2,4-dieniminium cation, photoisomerization

1 | INTRODUCTION

Photoswitches constitute a class of molecular machines that undergo reversible isomerization upon stimulus by light, so-called photoisomerization. Computational approaches for photoisomerization processes are considered to be of great value for the study of photoswitches, especially in conjunction with spectroscopic techniques.[1–3] To get a more complete overview of the isomerization mechanism itself and the interplay of several electronic states, accurate ab initio molecular dynamics are needed. However, the computational costs of such calculations are high, and they are complicated by the frequent occurrence of conical intersections,[4] which require special attention to the chosen method. From ground and excited state electronic structure calculations, the mechanism itself cannot be fully elucidated, but electronic structure theory provides valuable information about the potential energy surfaces and may indicate possible reaction paths for the isomerization process.

Many features of the potential energy surface are important for the machinery of photoswitches. Ground state surfaces give information on relative stability of isomers, relaxation processes following decay from excited state and energy barriers for thermal isomerization. The energy barriers will indicate whether a molecule may

function as a photoswitch at all (high enough energy barrier in one direction) and if the process is thermally reversible. Excited states naturally play a key role in the mechanisms of photoisomerization, with curvature and shapes giving information on the efficiency of possible decay pathways to the ground state and whether the process is photochemically reversible. The energy of the excited states relative to the ground state energy will give information on wavelengths needed for initiating (and for certain photoswitches, reversing) the isomerization process. Mapping out potential energy surfaces for ground and excited states can also yield information on and characterize conical intersections, depending on the choice of method.

Due to the occurrence of conical intersections and near-degenerate states in photoisomerization processes, multiconfigurational self-consistent field methods, such as the complete active space SCF (CASSCF)[5] methods, as well as multireference methods including dynamical electron correlation, such as multireference configuration interaction with singles and doubles (MRCISD),[6] MRCISD with a Davidson-type correction (MRCISD+Q),[7,8] (multi-state) complete active space second order perturbation theory (CASPT2)[9,10] with and without a ionization potential - electron affinity shift (IPEA),[11] restricted active space second order perturbation theory (RASPT2),[12] (quasi-degenerate) n-electron valence state second order perturbation theory (NEVPT2),[13–15] and extended multiconfiguration quasi degenerate second order perturbation theory (XMCQDPT2),[16] have been used extensively.[1,17–33] Single-reference methods such as time dependent density functional theory (TDDFT),[34] Møller–Plesset perturbation theory,[35] and various members of the coupled cluster hierarchy of wave function models, have also been used.[24,36–44] One advantage of single-reference methods compared to multireference methods is that no active space selection is necessary. Hence, the quality of the results will not depend on whether the appropriate orbital space has been chosen by the user. Furthermore, although single-reference coupled cluster methods cannot describe near-degeneracies, coupled cluster models with at least triples excitations can describe electronic states with doubly excited character that are important for organic photochemistry. For this purpose, approximate triples schemes such as the iterative CC3 model,[45] or the non-iterative equation-of-motion (EOM) CCSD(dT), EOM-CCSD(fT)[46–48] and EOM-CCSD(T)(a)/EOM-CCSD(T)(a)*[49] models can be used in place of CCSDT.[50] However, for excited electronic states dominated by single-electron excitations, low-level truncations of the hierarchy, for example, CCSD[51] or approximate versions such as CC2,[52] can be used. Hence, the adequacy of coupled cluster models for photoswitches will depend on the chosen truncation level.

The coupled cluster Jacobian, which is diagonalized to obtain excited states, is nonsymmetric and may become defective at conical intersections.[53] This precludes the standard models from being used for ab initio excited state dynamics of photochemical systems. However, coupled cluster has advantages for the characterization of ground and excited state surfaces, such as the inclusion of dynamical correlation and the possibility for systematic improvement offered by choice of truncation level. In addition, coupled cluster models are black box in nature and the user does not have to define active spaces or parameters. However, due to the computational cost of including triple (or approximate triple) excitations to the hierarchy, there are few such results for potential energy surfaces of photoswitches in the literature. A notable exception is the use of EOM spin-flip (SF) CCSD with perturbative triples corrections (EOM-SF-CCSD(dT) and EOM-SF-CCSD(fT)) for the penta-2,4-dieniminium cation (PSB3) model system of retinal, which shows excellent agreement with MRCISD+Q results.[54] The spin-flip approach exploits the fact that a high-spin triplet reference is well behaved across the bond torsion and generates singlet ground and excited states as spin-flip excitations from the triplet reference. From this study, it is clear that inclusion of triples leads to a significantly better agreement with MRCISD+Q compared to EOM-SF-CCSD; however, it is unclear whether the high-spin reference is necessary to obtain this accuracy. CC3 has also been used for the PSB3 system,[44] but without comparison to high-level multireference methods.

For PSB3, the extensive set of MRCISD+Q calculations by Olivucci and collaborators[27] have proven indispensable for benchmarking other computational methods.[54,55] Comparisons have been made between these MRCISD+Q results and EOM variants of coupled cluster such as EOM-CCSD, EOM-SF-CCSD, EOM-SF-CCSD (dT), and EOM-SF-CCSD(fT).[54] Based on this comparison, EOM-SF-CCSD(dt/ft) was shown to agree well with MRCISD+Q. The importance of dynamical electron correlation has also been shown for PSB3, where CASSCF gave a barrierless first singlet excited state (S_1) potential energy surface while CASPT2 yields an S_1 surface with a small barrier.[56] Introduction of dynamical correlation by performing single point calculations along the CASSCF S_1 surface did not correct the shape of the potential energy surface. In addition, Send et al.[44] investigated excited state surfaces generated by rotation around all bonds in PSB3 using TDDFT, CC2, and CC3. From their results, it appears that there are significant differences between the coupled cluster methods and TDDFT, particularly for rotations around single bonds.

Another photoswitch that has garnered much attention is azobenzene and its derivatives. Due to the size of azobenzene, limitations are imposed on choice of computational method and/or basis set. Zhu et al.[31,32] optimized equilibrium states, transition states and conical intersections with five state averaged (5SA) CASSCF (6,6)/6-31G,[57] for the ground state and the first three singlet excited states. The focus of the work in Reference 32 was primarily to carry out molecular dynamics, however, a rotational path was generated by interpolation, which can be used to compare other computational methods with CASSCF. It should be noted that the CASSCF excitation energies of the cis and trans structures in Refs. 31 and 32 deviate significantly from experimental values, which can be explained by the fact that CASSCF excitation energies have been found to have a large deviation from more accurate methods.[58] Recently, a thorough mapping of the ground state and first excited state potential energy surfaces of azobenzene was performed by Aleotti et al.[33] using RASPT2. In this case, the excitation energies of the cis and trans structures are in much better agreement with experimental values. This shows the importance of dynamical electron correlation when computing

excitation energies for comparison with experimental results. Casellas et al.[30] further argue that dynamical electron correlation must also be included for geometry optimization of critical points on the lowest singlet excited states. In addition to the studies mentioned, there are several studies of azobenzene using CASSCF and other multireference techniques containing dynamical electron correlation.[3,18,21–23,25,28,59] With respect to single-reference methods, CC2 and CCSD calculations of excitation energies have been performed for azobenzene by Hättig and coworkers.[38,39] However, high-level single-reference calculations with at least triples corrections are not presented in literature for azobenzene, and hence experimental results[60] provide the basis for evaluating computational results.

The focus of this article is to explore the capabilities of the coupled cluster models for mapping singlet potential energy surfaces of photoswitches. We utilize the newly released and efficient coupled cluster code in the eT program[61] to generate potential energy surfaces for CC2, CCSD, and CC3. As already mentioned, CC2 and CCSD will not give good results for excitations of strong doubly excited character, but for single-excitation dominated processes they are expected to give good results.[62] In this study, the performance of CC2, CCSD, and CC3 are presented for torsional angles that include potentially problematic regions such as isomerization points. The photoswitches studied are PSB3, which displays torsion of a C—C double bond, and azobenzene where we study the torsion about the N—N double bond. The large number of studies facilitates evaluation of the performance of the coupled cluster models. The advantage of CC3 is the fact that it can describe excitations of doubly excited character and that results are not complicated by choice of an active orbital space. With the new CC3 implementation (see, Reference 63) photoswitches of about 20 non-hydrogen atoms can be treated using augmented basis sets, such as aug-cc-pVDZ, using high performance computing resources. The inclusion of diffuse functions has been shown to significantly impact vertical excitation energies,[64] hence being able to perform CC3 calculations with augmented basis sets is valuable.

The article is structured as follows. In Section 2.1, we provide computational details. In Section 2.2, we present potential energy surfaces of PSB3 generated by CC2, CCSD, and CC3 and compare to MRCISD+Q[27] and spin-flip coupled cluster methods.[54] Further, we explore the basis set effect for the potential energy surfaces for PSB3. In Section 2.3, we explore how coupled cluster model, basis set, molecular geometry, and solvent effects affect vertical excitation energies for cis and trans ground state equilibrium azobenzene structures. Finally, CC3 potential energy surfaces for isomerization through CNNC torsion for azobenzene are presented in Section 2.4. Concluding remarks are given in Section 3.

2 | RESULTS AND DISCUSSION

2.1 | Computational details

In this section, the software and settings used for computations are presented. CC2, CCSD, and CC3 excitation energies were computed with the eT program.[61] All coupled cluster calculations presented are computed using frozen core. The decomposition of the electron repulsion integrals[65] threshold was set to 10^{-10}. The energy and gradient thresholds for Hartree–Fock and the energy and residual thresholds for the coupled cluster ground state were all set to 10^{-8}. The energy and residual threshold for the coupled cluster excited states were set to 10^{-4}. In coupled cluster calculations where the solvent effects of methanol were accounted for by a polarizable continuum model (PCM),[66] the static permittivity was set to 32.63, the optical permittivity was set to 1.758 and the probe radius was set to 1.855 Å.

2.2 | The penta-2,4-dieniminium cation (PSB3)

In this section, we discuss CC2, CCSD, and CC3 results for CASSCF optimized penta-2,4-dieniminium cation (PSB3) structures presented by Olivucci and collaborators.[27] The three relevant isomerization paths are depicted schematically in Figure 1. The charge transfer (CT) path and covalent/diradical (DIR) path are both rotational minimum energy paths connecting the transition states (TS_{CT} and TS_{DIR}) to the cis-reactant and trans-product. The paths differ in the character of the wave functions, with the DIR path being dominated by a covalent/diradical wave function along the entire isomerization path and the CT path being dominated by a charge transfer wave function close to TS_{CT}, but otherwise being dominated by a covalent/diradical wave function. For these two paths, calculations are performed for the transition states and eight geometries on either side of the transition state, with the dihedral angle in the range $\sim 82^{\circ}$–103°. The bond length alternation (BLA) path corresponds to a coordinate obtained by linear interpolation and extrapolation of the two transition state structures (TS_{CT} and TS_{DIR}) and intercepts a single conical intersection. The bond length alternation coordinate is defined as the difference between the average bond lengths of formal double and single bonds, and has a positive value at TS_{CT} and negative values at TS_{DIR}. For details, see Reference 27. These structures are well suited for testing the capabilities of the coupled cluster methods, since extensive literature on both multireference and equation of motion-coupled cluster (with and without spin-flip) exists. The MRCISD+Q/6-31G* results from Reference 27 are used as reference for evaluating the coupled cluster methods. Although 6-31G* is a rather small basis set for describing excited states, results in Reference 27 are presented for all paths using 6-31G*. It is, therefore, useful in the context of evaluating whether coupled cluster models can perform on par with MRCISD +Q. To assess the shape of surfaces generated by coupled cluster models, the nonparallelity value is computed for the S_0 and S_1 surfaces for all paths. The nonparallelity value is given by,

$$\Delta E_{max} - \Delta E_{min} \tag{1}$$

where ΔE_{max} and ΔE_{min} is the maximum and minimum energy difference for a potential energy surface computed in two different manners, respectively. Nonparallelity values are in Sections 2.2.1–2.2.3 used to evaluate the shape of the coupled cluster surfaces relative to the benchmark results. In Section 2.2.4, we use nonparallelity values

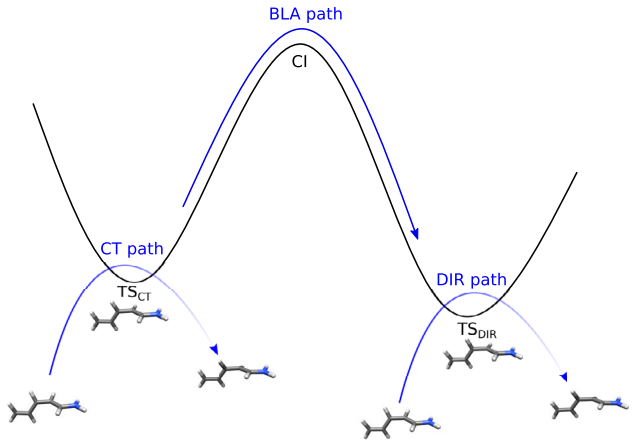

FIGURE 1 Schematic representation of the CT and DIR path, which are minimum energy paths in the cis → trans isomerization, and the BLA path, which is a path that interpolates the transition states of the CT and DIR paths

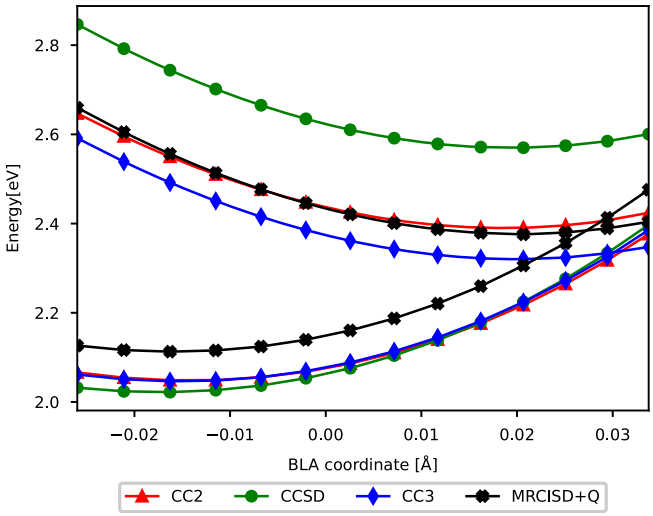

FIGURE 2 S_0 and S_1 energies for BLA-path relative to cis-PSB3 computed with CC2, CCSD and CC3 with 6-31G*. MRCISD+Q with 6-31G* benchmark results from Reference 27 are included for comparison

to evaluate how coupled cluster surfaces change upon changing the basis set.

2.2.1 | BLA path

In this section, we consider results for the BLA path using 6-31G*. CC2, CCSD, and CC3 results are plotted in Figure 2 together with the MRCISD+Q benchmark results of Reference 27, and energies are relative to cis-PSB3. Additionally, nonparallelity values of the coupled cluster models relative to MRCISD+Q are presented in Table 1. From Figure 2, we first of all see that CCSD cannot describe the BLA path. The deviation in vertical excitation energies relative to MRCISD+Q is found to vary between 0.13 and 0.28 eV. The conical intersection cannot be seen for the CCSD surfaces, as it is shifted beyond TS_{DIR} and outside the range of the plot. However, the nonparallelity values for the S_0 and S_1 surfaces for the BLA path computed with CCSD are only of 0.02 eV and 0.01 eV (see Table 1), so the shape of the S_0 and S_1 surfaces are similar to those from the MRCISD+Q benchmark results. This is consistent with EOM-CCSD results from Reference 54, where the nonparallelity values for the S_0 and S_1 surfaces where 0.02 eV and 0.01 eV, respectively. CC2 energies are closer to the MRCISD+Q reference values than CCSD, as is seen from both Figure 2 and by comparing vertical excitation energies. The conical intersection for CC2 is shifted closer to that of the MRCISD+Q relative to CCSD, although still beyond TS_{DIR} and outside of the plot. With respect to the vertical excitation energies, the CC2 results deviate between 0.02 and 0.11 eV from the MRCISD+Q results, which is smaller than the deviations for CCSD. However, the nonparallelity values are larger for CC2 than for CCSD, with a value of 0.04 eV for the S_0 surface and 0.03 eV for the S_1 surface. We see from Figure 2 that the CC3 results for the S_0 and S_1 surfaces appear to be quite similar to the MRCISD+Q results, except that they are shifted downward in energy by approximately 0.07 eV. The CC3 vertical excitation energies differ by only 0.01–0.03 eV compared to the MRCISD+Q results and the nonparallelity values are small, with a value of 0.03 eV for S_0 and 0.01 eV for S_1. Hence, the CC3 surfaces are similar to the MRCISD+Q surfaces, also with respect to the position of the conical intersection. CC3 also performs similarly to EOM-SF-CCSD(dT) from Reference 54, as can be seen from the nonparallelity values given in Table 1. CC3 shows a slightly better agreement for the S_0 surface, while for the S_1 surface the agreement depends on whether the nonparallelity value of EOM-SF-CCSD(dT) with or without kinks is used (see Reference 54). Small differences are also seen when comparing CC3 vertical excitation energy of TS_{CT} and TS_{DIR} with either EOM-SF-CCSD(dT) or EOM-SF-CCSD(fT) from Reference 54. For TS_{CT} the vertical excitation energy is 0.45 eV, 0.48 eV, and 0.43 eV, for CC3, EOM-SF-CCSD(dT), and EOM-SF-CCSD(fT), respectively. For TS_{DIR}, the vertical excitation energy is 0.05 eV, 0.03 eV, and 0.03 eV, for CC3, EOM-SF-CCSD(dT), and EOM-SF-CCSD(fT), respectively. Hence, we see that accurate results may be obtained without using a well-behaved high-spin triplet reference.

2.2.2 | CT path

In this section, we consider results for the CT path using 6-31G*. CC2, CCSD, and CC3 results are plotted in Figure 3 together with the MRCISD+Q benchmark results of Reference 27, and energies are relative to cis-PSB3. From Figure 3, we see that CCSD provides too large excitation energies, as was the case for the BLA path. The difference in vertical excitation energies between CCSD and MRCISD+Q is in the range 0.23–0.28 eV, which is similar to that of the BLA path (0.13–0.28 eV). However, CCSD is doing a worse job reproducing the

TABLE 1 The nonparallelity values for CC2, CCSD, CC3 for the S_0 and S_1 states along the DIR, CT and BLA paths, given in eV

Method	DIR S_0	CT S_0	BLA S_0	DIR S_1	CT S_1	BLA S_1
CC2	0.06	0.03	0.04	0.22	0.22	0.03
CCSD	0.16	0.14	0.02	0.11	0.10	0.01
CC3	0.06	0.03	0.03	0.03	0.04	0.01
EOM-SF-CCSD(dT)	0.06	0.02	0.06 (0.04)	0.03	0.02	0.04 (0.01)

Note: The nonparallelity values are computed relative to the MRCISD+Q/6-31G* benchmark results from Reference 27. Nonparallelity values for EOM-SF-CCSD(dT) are reproduced from Reference 54, where the values in parentheses are calculated by ignoring the kinks along the BLA path. The EOM-SF-CCSD(dT) used a restricted open shell Hartree–Fock reference state.

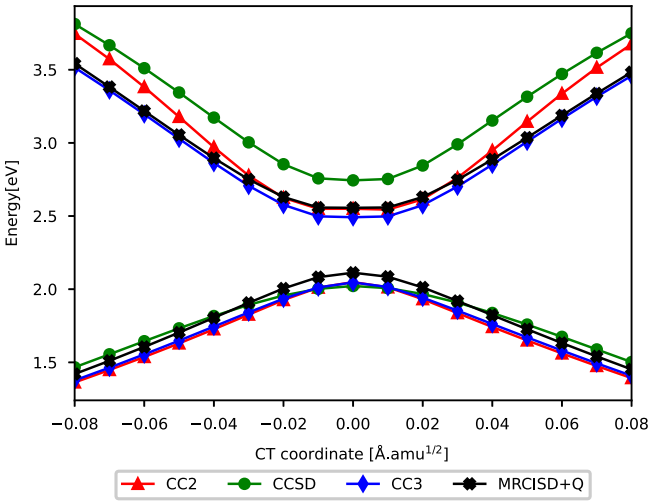

FIGURE 3 S_0 and S_1 energies for CT-path relative to cis-PSB3 computed with CC2, CCSD and CC3 with 6-31G*. MRCISD+Q with 6-31G* benchmark results from Reference 27 are included for comparison

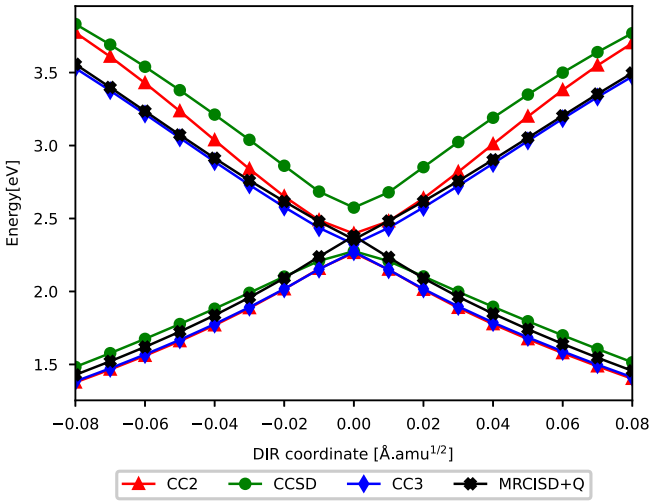

FIGURE 4 S_0 and S_1 energies for the DIR-path relative to cis-PSB3 computed with CC2, CCSD and CC3 with 6-31G*. MRCISD+Q with 6-31G* benchmark results from Reference 27 are included for comparison

shapes of the S_0 and S_1 surfaces than for the BLA path, as can be seen from the nonparallelity values (see Table 1). The nonparallelity values of the CT path with CCSD are one order of magnitude larger than for the BLA path for both surfaces. Considering the CC2 surfaces, we see from Figure 3 that CC2 provides a better agreement with MRCISD+Q for some of the vertical excitation energies than CCSD, with deviations ranging from 0.06 eV (close to CT coordinate 0.0) to 0.26 eV at CT coordinates ±0.08 Å·amu$^{1/2}$. CC2 has a nonparallelity value for the S_0 surface of 0.03 eV, whereas the nonparallelity value for S_1 surface is 0.22 eV. Hence, CC2 can reproduce the shape of the ground state, but not the first excited state. The improved performance of CC2 relative to CCSD for the S_0 surface is most likely due to error cancellations, since CC2 is an approximation of CCSD. CC3 yields results that are consistent with MRCISD+Q. As can be seen from Figure 3, both the S_0 and S_1 CC3 surfaces are close to the MRCISD+Q surfaces. The vertical excitation energies differ from the MRCISD+Q results by 0.01–0.03 eV, which is significantly less than the deviations for CCSD (0.23–0.28 eV) and CC2 (0.06–0.26 eV). The nonparallelity value of CC3 for the CT path is also small, with values of 0.03 eV for S_0 and 0.04 eV for S_1. Based on the nonparallelity value, CC3 performs slightly worse than EOM-SF-CCSD(dT) from Reference 54 for both states, but the nonparallelity values are still the same order of magnitude.

2.2.3 | DIR path

The results for the DIR path for CC2, CCSD and CC3 using 6-31G* are plotted in Figure 4 together with the MRCISD+Q benchmark results of Reference 27, and energies are relative to cis-PSB3. From Figure 4 we see that the CC2, CCSD, and CC3 results for the DIR path show much of the same characteristics as the CT path. CCSD displays too large vertical excitation energies, deviating between 0.22–0.28 eV, and surfaces, which deviate from the shapes of the MRCISD+Q surfaces (see Table 1). The CC2 S_0 surface has approximately the same shape as the MRCISD+Q S_0 surface, whereas larger deviations are found for the S_1 surface. The deviation for CC2 vertical excitation energies relative to MRCISD+Q varies between 0.08 eV (close to DIR coordinate 0.0) to 0.27 eV at DIR coordinates ±0.08 Å·amu$^{1/2}$. CC3 shows small deviations in excitation energies, between 0.02 and 0.04 eV, compared to MRCISD+Q, as well as small nonparallelity values for both

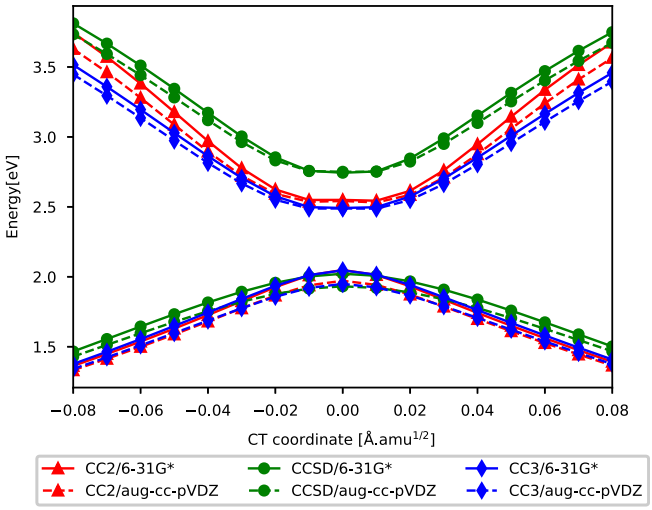

FIGURE 5 S_0 and S_1 energies for the CT path relative to cis-PSB3 computed with CC2, CCSD and CC3 with the 6-31G* and aug-cc-pVDZ basis sets

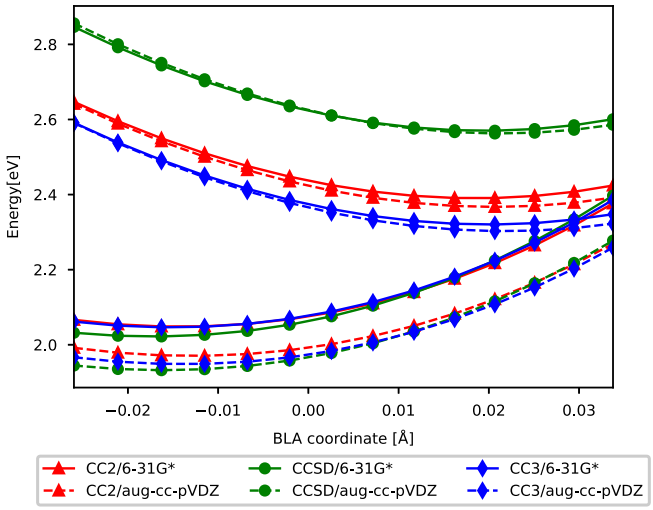

FIGURE 7 S_0 and S_1 energies for the BLA path relative to cis-PSB3 computed with CC2, CCSD and CC3 with the 6-31G* and aug-cc-pVDZ basis sets

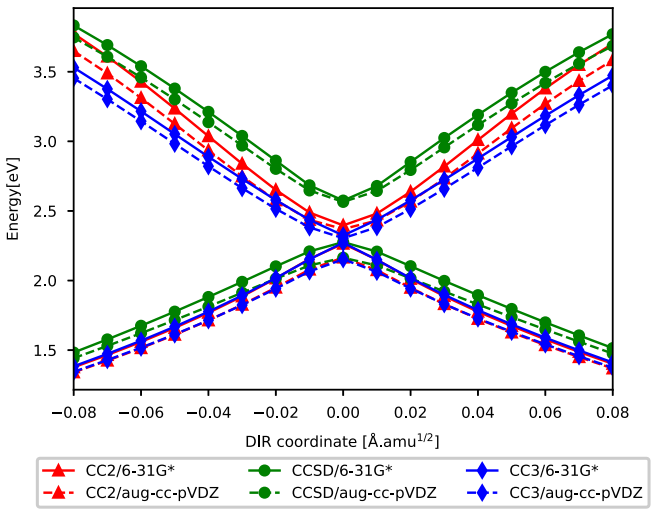

FIGURE 6 S_0 and S_1 energies for the DIR path relative to cis-PSB3 computed with CC2, CCSD and CC3 with the 6-31G* and aug-cc-pVDZ basis sets

surfaces. The nonparallelity values of CC3 and EOM-SF-CCSD (dT) from Reference 54 are equal for both surfaces.

2.2.4 | Basis set considerations

Most results presented for PSB3 in the literature are generated using 6-31G*. In the previous sections, we presented the performance of CC2, CCSD, and CC3 relative to MRCISD+Q, all using 6-31G*. We note that basis set effects for MRCISD+Q was explored in Reference 27 for the BLA path using Pople basis sets. In this section, we study the basis set dependence for coupled cluster calculations. We choose to extend from using 6-31G* to the correlation consistent basis set

TABLE 2 The nonparallelity values for CC2, CCSD, CC3 for the S_0 and S_1 states along the DIR, CT and BLA paths, using aug-cc-pVDZ. All energies are given in eV

Method	DIR S_0	CT S_0	BLA S_0	DIR S_1	CT S_1	BLA S_1
CC2	0.07	0.05	0.03	0.10	0.11	0.03
CCSD	0.07	0.06	0.03	0.08	0.09	0.02
CC3	0.08	0.06	0.03	0.06	0.06	0.02

Note: The nonparallelity values are computed relative to the CC2, CCSD, and CC3 results using 6-31G*.

aug-cc-pVDZ rather than staying within the Pople basis set hierarchy, since Dunning's correlation consistent basis sets are seen to converge faster with respect to correlation energy than the Pople basis sets.[67] In Figures 5–7, we present the 6-31G* coupled cluster results from Figures 2–4 together with results generated using aug-cc-pVDZ. The effects of increasing the basis set on the CT path (Figure 5) and the DIR path (Figure 6) are similar. The excited state is shifted to lower energies at large absolute coordinates, whereas the ground state is shifted to lower energies around coordinate 0.0 Å·amu$^{1/2}$. For CC2 the largest shift is found close to 0.0 Å·amu$^{1/2}$, with the ground state being shifted 0.08 eV for the CT path and 0.10 eV for the DIR path. For the BLA path (Figure 7), the change of basis to aug-cc-pVDZ shifts the ground state energy (relative to cis-PSB3) for all three methods by 0.08–0.11 eV. For the excited state, the shift is smaller, as seen from Figure 7. In Table 2, the nonparallelity values of the aug-cc-pVDZ calculations relative to the 6-31G* coupled cluster calculations are presented and demonstrate how much the shape of the surface is affected by choice of basis set. We see from Table 2 that, although the ground state is lowered in energy, the shape of the ground and excited state for the BLA path is least affected by change of basis. The effect is similar for all coupled cluster models used, with the nonparallelity values being 0.03 eV for the ground state and 0.02–

0.03 eV for the excited state. This is also what is seen for MRCISD+Q results in Reference 27. The ground and excited states for CT and DIR paths are more affected by the choice of basis than the BLA path, as seen from Figures 5 and 6 and the nonparallelity values.

2.3 | Exploring vertical excitation energies for ground state equilibrium cis- and trans-azobenzene

In this section we investigate how choice of coupled cluster method and basis set, as well as accounting for solvent, affects computed $S_0 \rightarrow S_1$ and $S_0 \rightarrow S_2$ vertical excitation energies for the azobenzene molecule (see Figure 8). CC2 and CC3 vertical excitation energies are computed for two sets of cis and trans equilibrium structures to also illustrate the effect the molecular geometry has on the vertical excitation energies. The structures used are the 5SA-CASSCF(6,6)/6-31G optimized structures from Reference 32 (denoted cis[a] and trans[a]) and MP2/aug-cc-pVDZ optimized structures (denoted cis[b] and trans[b]). CC2 results are computed using cc-pVDZ, aug-cc-pVDZ, cc-pVTZ and aug-cc-pVTZ, whereas CC3 results are computed using cc-pVDZ and aug-cc-pVDZ. For calculations using aug-cc-pVDZ and aug-cc-pVTZ augmentation is only added to non-hydrogen atoms (using cc-pVDZ and cc-pVTZ on hydrogen). The vertical excitation energies are presented in Table 3 together with experimental UV–VIS results.[60] A discussion in connection to the experimental results is provided at the end of this section.

We first compare CC2 and CC3 results. The absolute difference between CC2 and CC3 $S_0 \rightarrow S_1$ excitation energies when the same basis set is used is 0.00–0.02 eV, whereas the absolute difference between CC2 and CC3 $S_0 \rightarrow S_2$ excitation energies is 0.04–0.10 eV. The slightly larger difference between CC2 and CC3 for the $S_0 \rightarrow S_2$ transition relative to the $S_0 \rightarrow S_1$ transition, may be due to the S_2 state having a lower fraction of single amplitudes and hence CC3 provides a better description. The fraction of singles in the CC3 calculations for cis[a] and trans[a] are listed in Table 4 (together with fraction of singles for the rotational path discussed in Section 2.4). However, the differences between CC2 and CC3 are still small for the structures studied in this section, and this is consistent with available benchmark literature.[62]

From Table 3, we see that the choice of basis set impacts excitation energies for $S_0 \rightarrow S_1$ differently than $S_0 \rightarrow S_2$ for both sets of structures. Improving the basis set from cc-pVDZ to aug-cc-pVDZ lowers both excitation energies for all structures and methods. For CC2, the $S_0 \rightarrow S_1$ excitation energies are lowered by between 0.04 eV (for trans[a]) and up to 0.06 eV (for cis[b]). Changes in $S_0 \rightarrow S_1$ excitation energies for CC3 when improving from cc-pVDZ to aug-cc-pVDZ are seen to be in the same range (0.02–0.06 eV). In contrast to the $S_0 \rightarrow S_1$ excitation energies, the $S_0 \rightarrow S_2$ excitation energies are seen to change significantly upon improving the basis set from cc-pVDZ to aug-cc-pVDZ. The largest change for CC2 is 0.22 eV (for trans[a] and trans[b]) and the largest change for CC3 is 0.23 eV (trans[b]). Improving the basis set from cc-pVDZ to cc-pVTZ also lowers the excitation energies for all structures. The $S_0 \rightarrow S_1$ excitation is lowered in the range 0.06–0.07 eV, whereas the $S_0 \rightarrow S_2$ excitation energy is lowered in the range 0.13–0.17 eV. Hence, cc-pVTZ lowers the $S_0 \rightarrow S_1$ transition more and $S_0 \rightarrow S_2$ transition less than does aug-cc-pVDZ. We see from the CC2 results that increasing the basis set from aug-cc-pVDZ to aug-cc-pVTZ lowers the $S_0 \rightarrow S_1$ excitation energies by 0.03–0.05 eV, whereas the $S_0 \rightarrow S_2$ excitation energies are lowered by 0.01–0.04 eV. In contrast, increasing the basis set from cc-pVTZ to aug-cc-pVTZ, the $S_0 \rightarrow S_1$ excitation energy is lowered by 0.02–0.04 eV, whereas the $S_0 \rightarrow S_2$ excitation energy is lowered by 0.06–0.09 eV. Hence, $S_0 \rightarrow S_1$ and $S_0 \rightarrow S_2$ excitations seems to have different basis set requirements, with $S_0 \rightarrow S_2$ excitations being more sensitive to the inclusion of diffuse functions.

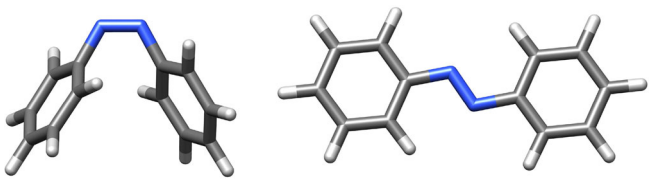

FIGURE 8 Cis (left) and trans (right) isomers of azobenzene

TABLE 3 CC2 and CC3 vertical excitation energies calculated for cis- and trans-azobenzene structures optimized with CASSCF/6-31G[32] (superscript *a*) and cis- and trans-azobenzene structures optimized with MP2/aug-cc-pVDZ (superscript *b*). All energies are given in eV

		CC2				CC3		
Structure	Transition	DZ	aDZ	TZ	aTZ	DZ	aDZ	UV–VIS[60]
Cis[a]	$S_0 \rightarrow S_1$	2.78	2.73	2.72	2.70	2.77	2.73	2.88
	$S_0 \rightarrow S_2$	4.71	4.52	4.58	4.51	4.62	4.48	4.43
Trans[a]	$S_0 \rightarrow S_1$	2.72	2.68	2.66	2.64	2.72	2.70	2.80
	$S_0 \rightarrow S_2$	4.56	4.34	4.39	4.30	4.61	4.42	3.92
Cis[b]	$S_0 \rightarrow S_1$	3.18	3.12	3.11	3.08	3.17	3.11	2.88
	$S_0 \rightarrow S_2$	4.61	4.45	4.47	4.41	4.55	4.41	4.43
Trans[b]	$S_0 \rightarrow S_1$	2.94	2.89	2.87	2.84	2.94	2.91	2.80
	$S_0 \rightarrow S_2$	4.20	3.98	4.03	3.94	4.30	4.07	3.92

Note: The basis set used for CC2 are cc-pVDZ, cc-pVTZ, aug-cc-pVDZ and aug-cc-pVTZ (cc-pVDZ and aug-cc-pVDZ for CC3). In addition, energies from UV–VIS spectroscopy performed in methanol[60] for cis- and trans-azobenzene are presented.

TABLE 4 Fraction of singles amplitudes, $|\mathbf{R}_1|/|\mathbf{R}|$, for the first and second excited states calculated with CC3/cc-pVDZ for the CASSCF/6-31G azobenzene structures from Zhu et al.[32]

Dihedral angle (degrees)	S_1	S_2
9.5 (cis[a])	0.96	0.92
30	0.96	0.91
50	0.96	0.68
70	0.96	0.38
90	0.95	0.05
110	0.93	0.13
130	0.96	0.44
150	0.95	0.91
180 (trans[a])	0.95	0.93

TABLE 5 CC2 and CC3 vertical excitation energies calculated with cc-pVDZ and aug-cc-pVDZ, where methanol solvent effects are accounted for by the PCM model (see Section 2.1 for PCM specifications). All energies are given in eV

		CC2		CC3
Structure	Transition	DZ	aDZ	DZ
Cis[a]	$S_0 \rightarrow S_1$	2.90	2.85	2.90
	$S_0 \rightarrow S_2$	4.72	4.54	4.63
Trans[a]	$S_0 \rightarrow S_1$	2.78	2.74	2.78
	$S_0 \rightarrow S_2$	4.51	4.28	4.58
Cis[b]	$S_0 \rightarrow S_1$	3.26	3.18	3.25
	$S_0 \rightarrow S_2$	4.55	4.36	4.51
Trans[b]	$S_0 \rightarrow S_1$	2.98	2.93	2.98
	$S_0 \rightarrow S_2$	4.16	3.93	4.26

From the results in Table 3 we can also discuss excitation energies for two different cis- and trans-geometries, that is, 5SA-CASSCF (6,6)/6-31G ground state optimized structures from Reference 32 (cis[a] and trans[a]) and MP2/aug-cc-pVDZ ground state optimized structures (cis[b] and trans[b]). A notable difference between the cis-structures is the CNNC dihedral angles, which is 9.5° for cis[a] and 6.0° for cis[b]. For the trans structures a notable difference is the NNC bond angles, which are 117.9° and 118.2° for trans[a] and 113.3° for both angles for trans[b]. For simplicity, we only discuss CC2/aug-cc-pVTZ results, but we note that the trends observed for CC2/aug-cc-pVTZ is seen for all basis sets and also for CC3 results. For cis[a] and cis[b], the differences in excitation energies are 0.38 eV for $S_0 \rightarrow S_1$ and 0.10 eV for $S_0 \rightarrow S_2$. For the trans[a] and trans[b] structures, the differences in excitation energies are 0.20 eV for $S_0 \rightarrow S_1$ and 0.36 eV for $S_0 \rightarrow S_2$. The differences between the sets of cis- and trans-structures are, therefore, significant. When we proceed to discuss and compare against experimental results we will only consider the MP2/aug-cc-pVDZ structures (cis[b] and trans[b]). We expect MP2/aug-cc-pVDZ optimized structures to be more representative gas phase ground state structures than the ones generated using 5SA-CASSCF(6,6)/6-31G (cis[a] and trans[a]) due to the inclusion of dynamical correlation and the use of a larger basis set.

Here, we compare computed results against absorption maxima from UV–VIS spectroscopy in methanol taken from Reference 60, which are also presented in Table 3. When comparing the computed vertical excitation energies to absorption maxima, we keep in mind that an absorption maximum does not necessarily represent a vertical transition, depending on how fast nuclear rearrangement occurs. We make a rough estimate at what can be considered good agreement with experiment by considering available literature. A study conducted by Bai et al.[68] showed an average deviation of 0.11 ± 0.08 eV between CC2 vertical excitations and absorption maxima computed using a nuclear ensemble approach at the CC2 level for a set of 28 molecules (60 transitions) to account for nuclear rearrangement. Based on this, as well as errors related to the methods used,[62] we discuss the results based on the assumption that a deviation of 0.10 eV, or less, relative to the absorption maximum constitutes reasonable agreement with experiments. However, we further note that the experimental results are obtained in solution and hence both direct solvent effects and geometry will impact the results. The comparison with absorption maxima will be made for the theoretically best results, that is, CC2/aug-cc-pVTZ and CC3/aug-cc-pVDZ calculations for the cis[b] and trans[b] structures. The CC2/aug-cc-pVTZ results show good agreement for both transition of trans[b], overestimating the $S_0 \rightarrow S_1$ transition by 0.04 eV and overestimating the $S_0 \rightarrow S_2$ transition by 0.02 eV. The agreement is worse for the cis[b] $S_0 \rightarrow S_1$ transition, which is overestimated by 0.20 eV, while the cis[b] $S_0 \rightarrow S_2$ transition is in good agreement, being underestimated by 0.02 eV. It should be noted that there are differences observed when comparing our results to the CC2/aug-cc-pVTZ results presented in Reference 39. For example, their $S_0 \rightarrow S_1$ excitation energy for cis-azobenzene overestimates the absorption maximum by 0.12 eV. These difference can be explained by structural differences, as the CNNC dihedral angle of their cis-azobenzene structure deviates by 1.3° compared to the cis[b]. This further illustrates the effect structure has on vertical excitation energies.

Comparing CC3/aug-cc-pVDZ results to absorption maxima, the $S_0 \rightarrow S_1$ transition of cis[b] is overestimated by 0.23 eV, while the $S_0 \rightarrow S_2$ transition of cis[b] is underestimated by 0.02 eV. For trans[b], the $S_0 \rightarrow S_1$ transition is overestimated by 0.11 eV, while the $S_0 \rightarrow S_2$ is overestimated by 0.15 eV. Thus, CC3/aug-cc-pVDZ shows a similar agreement with absorption maxima as CC2/aug-cc-pVTZ for cis[b], while the agreement for trans[b] is worse. The worse agreement for the $S_0 \rightarrow S_1$ of trans[b] appears to be mainly due to the basis set effect, since CC2/aug-cc-pVDZ and CC3/aug-cc-pVDZ results only differ by 0.02 eV. However, the $S_0 \rightarrow S_2$ transition of trans[b] can only be explained by inherent differences between CC2 and CC3, since CC2/aug-cc-pVDZ and CC3/aug-cc-pVDZ results differ by 0.09 eV.

Another factor which must be considered when comparing vertical excitation energies with UV–VIS absorption maxima is the solvent effect. In Table 5, we present results for CC2/cc-pVDZ, CC2/aug-cc-pVDZ, and CC3/cc-pVDZ where methanol solvent effects are incorporated through PCM (see Section 2.1). The effect of including PCM

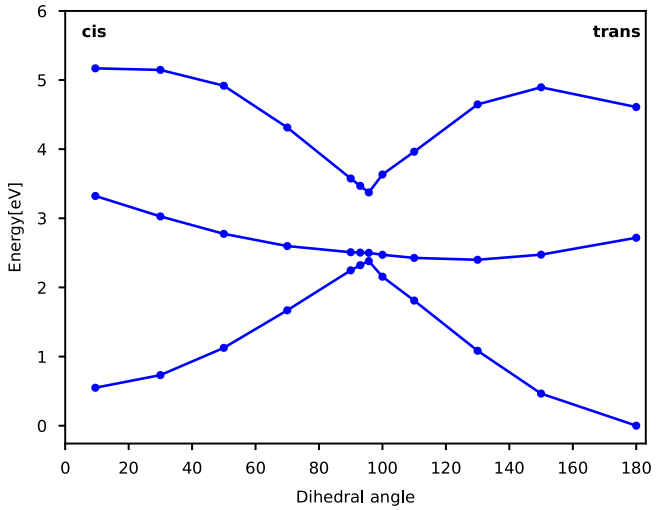

FIGURE 9 Ground state (S_0) and the two lowest excited singlet states (S_1, S_2) calculated with CC3 using cc-pVDZ, for a selected set of azobenzene structures along the rotational path from Reference 32

for these methods and basis set, is that the $S_0 \rightarrow S_1$ energies increase by 0.04–0.08 eV, while the $S_0 \rightarrow S_2$ transitions are lowered by 0.04–0.09 eV. The inclusion of solvent effects through PCM, therefore, does not appreciably improve the agreement between the computed vertical excitation energies and absorption maxima.

2.4 | Coupled cluster results for a rotational path of azobenzene including an excited state with doubly excited character

In this section, we discuss CC3 results for a cis to trans CNNC-rotational path obtained from Zhu et al.[32] The path consists of the cis and trans ground state structures, a twisted minimum energy structure optimized for the second excited state (rot-S2), all optimized with 5SA-CASSCF(6,6)/6-31G, and structures generated by linear interpolation of internal coordinates (LIIC) with respect to these three structures (for details see Reference 32). In Figure 9, CC3 results using the cc-pVDZ basis set are presented for selected structures along the described rotational path for the ground state and the states corresponding to the two lowest singlet vertical excitation energies. The maximum of S_0 corresponds to the aforementioned rot-S2 structure. To describe these states accurately, either cc-pVTZ, aug-cc-pVDZ or a bigger basis set should ideally be used, as can be seen from the basis set study of cis- and trans-azobenzene presented in Section 2.3. However, cc-pVDZ is sufficient to evaluate whether CC3 can describe these states.

Comparing to the results of Reference 32, it is seen that CC3 and 5SA-CASSCF(6,6) are in qualitative agreement for the ground and lowest excited state. However, for S_2, we see from Figure 9 that the CC3 results yield an energy barrier when going from the trans-isomer (180° dihedral angle) toward rot-S2. The barrier is absent in the CASSCF results of Zhu et al. Further, CC3 results for S_2 are reasonably flat in the region from a dihedral angle of 9.5° (cis-isomer) to between 30 and 50° before it rapidly decreases toward the minimum at rot-S2. The 5SA-CASSCF(6,6) results of Reference 32 predict an even decrease of the S_2 energy from cis to rot-S_2. Investigating the amplitudes of the CC3 calculations shows that in the region between 30–50° and 130–150° dihedral angle, the $\pi\pi^*$ state and the $n^2\pi^{*2}$ state switch ordering. At equilibrium structures the second excited state is the $\pi\pi^*$ state and in a broad region (approximately from 50 to 130° dihedral angle) around rot-S2, the $n^2\pi^{*2}$ state is the second excited state. The significant doubly excited character of the second excited state in this region is seen from the relative importance of singles amplitudes in the CC3 calculation. In Table 4 the fraction of singles amplitudes ($|\mathbf{R}_1|/|\mathbf{R}|$) is shown for the first and second excited state throughout the rotational path. As $\pi\pi^*$ and $n^2\pi^{*2}$ switch ordering, Table 4 shows a clear drop in fraction of singles amplitudes for the second excited state. Hence, for a qualitatively correct result for the second excited state in this region, triple excitations must be accounted for. In regions around the ground state equilibrium structures (cis and trans regions), the fraction of singles amplitudes is large, and lower levels of theory such as the CC2 model are sufficient as seen in Section 2.3. These results are consistent with the results in Reference 30 where $n\pi^*$, $\pi\pi^*$ and $n^2\pi^{*2}$ are computed at the multistate CASPT2 level along a rotational path for azobenzene. The results in Reference 30 show a crossing of $\pi\pi^*$ and $n^2\pi^{*2}$ at approximately 35° and 130° dihedral angle.

3 | CONCLUSIONS

The results for PSB3 showed that vertical excitation energies computed with CC2 and CCSD deviated from MRCISD+Q results by 0.02–0.27 eV and 0.13–0.28 eV, respectively. The nonparallelity values also showed that CCSD generally gave deviation in the shape of the surfaces relative to MRCISD+Q, and while the nonparallelity values were small for the CC2 ground states, larger nonparallelity values were found for the CC2 excited states. Contrary, CC3 provided excellent agreement with MRCISD+Q, with vertical excitation energies differing by 0.01–0.04 eV. As a consequence, the nonparallelity values for all ground and excited states were low. The performance of CC3 was similar to EOM-SF-CCSD (dT) presented in Reference 54, where it was seen that triples corrections are necessary. However, it appears that the use of a well-behaved triplet reference state was not required for the PSB3 surfaces explored here.

For equilibrium geometries of cis- and trans-azobenzene, a study of $S_0 \rightarrow S_1$ and $S_0 \rightarrow S_2$ vertical excitation energies computed by coupled cluster models was conducted. It was shown that the molecular geometry had the largest impact, yielding significant variations for vertical excitation energies and shifting the energy of S_1 and S_2 relative to each other. Further, a basis set of sufficient quality was required to describe these states. Both cc-pVTZ and aug-cc-pVDZ were shown to significantly change the vertical excitation energies relative to cc-pVDZ. However, aug-cc-pVDZ was shown to be the better choice of the two, since the inclusion of diffuse functions was found to be important to correctly describe $S_0 \rightarrow S_2$ transitions.

Conversely, the differences between CC2 and CC3 results were shown to be small. By comparing computed vertical excitation energies to UV–VIS absorption maxima, CC2/aug-cc-pVTZ results were found to agree well for all excitations, except the $S_0 \rightarrow S_1$ transition of cis-azobenzene. The computed vertical excitation energies were seen to be sensitive to molecular geometry, and this could in part explain the discrepancy between experimental and computational results. In the case of the CNNC rotational path from Reference 32, we presented the S_0, S_1, and S_2 surfaces using CC3. The CC3 S_0 and S_1 surfaces were in qualitative agreement with the CASSCF surfaces, while the S_2 surface differed significantly since $\pi\pi^*$ and $n^2\pi^{*2}$ switched ordering. This was seen from the onset of significant doubly excited character of the S_2 state in regions of the path. Hence, CC2 and CCSD would not be able to describe the region of the S_2 surface surrounding rot-S2, where $n^2\pi^{*2}$ was the second excited state.

Thus, the article has demonstrated that the coupled cluster models, despite being predominantly single-reference, constitute valuable tools for preliminary and simple black box studies of photoswitchable systems.

ACKNOWLEDGMENTS

The authors acknowledge computing resources through UNINETT Sigma2 the National Infrastructure for High Performance Computing and Data Storage in Norway through project numbers nn9409k. H.K, I-M.H. and R.H.M acknowledge funding from the Research Council of Norway through FRINATEK projects 263110 and 275506. A.C.P and H.K acknowledge funding from the Marie Skłodowska-Curie European Training Network "COSINE – COmputational Spectroscopy In Natural sciences and Engineering," Grant Agreement No. 765739.

DATA AVAILABILITY STATEMENT

xyz-coordinates for cis[b] and trans[b] azobenzene structures of Section 2.3 are given in Supporting Information.

ORCID

Ida-Marie Høyvik https://orcid.org/0000-0002-1239-7776

REFERENCES

[1] M. Quick, A. L. Dobryakov, M. Gerecke, C. Richter, F. Berndt, I. N. Ioffe, A. A. Granovsky, R. Mahrwald, N. P. Ernsting, S. A. Kovalenko, *J. Phys. Chem. B* **2014**, *118*, 8756.
[2] E. Tan, S. Amirjalayer, S. Smolarek, A. Vdovin, F. Zerbetto, W. Buma, *Nat. Commun.* **2015**, *6*, 5860.
[3] A. Nenov et al., *J. Phys. Chem. Lett.* **2018**, *9*, 1534.
[4] M. Robb, F. Bernardi, M. Olivucci, *Pure Appl. Chem.* **1995**, *67*, 783.
[5] B. O. Roos, P. R. Taylor, P. E. Siegbahn, *Chem. Phys.* **1980**, *48*, 157.
[6] R. J. Buenker, S. D. Peyerimhoff, W. Butscher, *Mol. Phys.* **1978**, *35*, 771.
[7] S. R. Langhoff, E. R. Davidson, *Int. J. Quantum Chem.* **1974**, *8*, 61.
[8] W. Duch, G. H. F. Diercksen, *J. Chem. Phys.* **1994**, *101*, 3018.
[9] K. Andersson, P. Malmqvist, B. O. Roos, *J. Chem. Phys.* **1992**, *96*, 1218.
[10] J. Finley, P. Åke Malmqvist, B. O. Roos, L. Serrano-Andrés, *Chem. Phys. Lett.* **1998**, *288*, 299.
[11] G. Ghigo, B. O. Roos, P. Åke Malmqvist, *Chem. Phys. Lett.* **2004**, *396*, 142.
[12] P. Å. Malmqvist, K. Pierloot, A. R. M. Shahi, C. J. Cramer, L. Gagliardi, *J. Chem. Phys.* **2008**, *128*, 204109.
[13] C. Angeli, R. Cimiraglia, S. Evangelisti, T. Leininger, J.-P. Malrieu, *J. Chem. Phys.* **2001**, *114*, 10252.
[14] C. Angeli, S. Borini, M. Cestari, R. Cimiraglia, *J. Chem. Phys.* **2004**, *121*, 4043.
[15] C. Angeli, M. Pastore, R. Cimiraglia, *Theor. Chem. Acc.* **2007**, *117*, 743.
[16] A. A. Granovsky, *J. Chem. Phys.* **2011**, *134*, 214113.
[17] M. Garavelli, T. Vreven, P. Celani, F. Bernardi, M. A. Robb, M. Olivucci, *J. Am. Chem. Soc.* **1998**, *120*, 1285.
[18] T. Ishikawa, T. Noro, T. Shoda, *J. Chem. Phys.* **2001**, *115*, 7503.
[19] L. De Vico, C. S. Page, M. Garavelli, F. Bernardi, R. Basosi, M. Olivucci, *J. Am. Chem. Soc.* **2002**, *124*, 4124.
[20] C. S. Page, M. Olivucci, *J. Comput. Chem.* **2003**, *24*, 298.
[21] E. Wei-Guang Diau, *J. Phys. Chem. A* **2004**, *108*, 950.
[22] A. Cembran, F. Bernardi, M. Garavelli, L. Gagliardi, G. Orlandi, *J. Am. Chem. Soc.* **2004**, *126*, 3234.
[23] L. Gagliardi, G. Orlandi, F. Bernardi, A. Cembran, M. Garavelli, *Theor. Chem. Acc.* **2004**, *111*, 363.
[24] M. Wanko, M. Hoffmann, P. Strodel, A. Koslowski, W. Thiel, F. Neese, T. Frauenheim, M. Elstner, *J. Phys. Chem. B* **2005**, *109*, 3606.
[25] I. Conti, M. Garavelli, G. Orlandi, *J. Am. Chem. Soc.* **2008**, *130*, 5216.
[26] G. Tiberio, L. Muccioli, R. Berardi, C. Zannoni, *ChemPhysChem* **2010**, *11*, 1018.
[27] S. Gozem, M. Huntress, I. Schapiro, R. Lindh, A. A. Granovsky, C. Angeli, M. Olivucci, *J. Chem. Theory Comput.* **2012**, *8*, 4069.
[28] Y. Harabuchi, M. Ishii, A. Nakayama, T. Noro, T. Taketsugu, *J. Chem. Phys.* **2013**, *138*, 064305.
[29] E. Walczak, B. Szefczyk, T. Andruniów, *J. Chem. Theory Comput.* **2013**, *9*, 4915.
[30] J. Casellas, M. J. Bearpark, M. Reguero, *ChemPhysChem* **2016**, *17*, 3068.
[31] L. Yu, C. Xu, C. Zhu, *Phys. Chem. Chem. Phys.* **2015**, *17*, 17646.
[32] C. Xu, L. Yu, F. L. Gu, C. Zhu, *Phys. Chem. Chem. Phys.* **2018**, *20*, 23885.
[33] F. Aleotti, L. Soprani, A. Nenov, R. Berardi, A. Arcioni, C. Zannoni, M. Garavelli, *J. Chem. Theory Comput.* **2019**, *15*, 6813.
[34] E. Runge, E. K. U. Gross, *Phys. Rev. Lett.* **1984**, *52*, 997.
[35] C. Møller, M. S. Plesset, *Phys. Rev.* **1934**, *46*, 618.
[36] P.-O. Åstrand, P. S. Ramanujam, S. Hvilsted, K. L. Bak, S. P. A. Sauer, *J. Am. Chem. Soc.* **2000**, *122*, 3482.
[37] N. Kurita, T. Ikegami, Y. Ishikawa, *Chem. Phys. Lett.* **2002**, *360*, 349.
[38] C. Hättig, K. Hald, *Phys. Chem. Chem. Phys.* **2002**, *4*, 2111.
[39] H. Fliegl, A. Köhn, C. Hättig, R. Ahlrichs, *J. Am. Chem. Soc.* **2003**, *125*, 9821.
[40] C. R. Crecca, A. E. Roitberg, *J. Phys. Chem. A* **2006**, *110*, 8188.
[41] R. Send, D. Sundholm, *J. Phys. Chem. A* **2007**, *111*, 27.
[42] R. Send, D. Sundholm, *J. Phys. Chem. A* **2007**, *111*, 8766.
[43] S. Yuan, Y. Dou, W. Wu, Y. Hu, J. Zhao, *J. Phys. Chem. A* **2008**, *112*, 13326.
[44] R. Send, D. Sundholm, M. P. Johansson, F. Pawłowski, *J. Chem. Theory Comput.* **2009**, *5*, 2401.
[45] H. Koch, O. Christiansen, P. Jørgensen, A. Merás, T. Helgaker, *J. Chem. Phys.* **1997**, *106*, 1808.
[46] P. Piecuch, M. Włoch, *J. Chem. Phys.* **2005**, *123*, 224105.
[47] P. U. Manohar, A. I. Krylov, *J. Chem. Phys* **2008**, *129*, 194105.
[48] P. U. Manohar, J. F. Stanton, A. I. Krylov, *J. Chem. Phys* **2009**, *131*, 114112.
[49] D. A. Matthews, J. F. Stanton, *J. Chem. Phys.* **2016**, *145*, 124102.
[50] J. Noga, R. J. Bartlett, *J. Chem. Phys.* **1987**, *86*, 7041.
[51] G. Purvis III., R. Bartlett, *J. Chem. Phys.* **1982**, *76*, 1910.
[52] O. Christiansen, H. Koch, P. Jørgensen, *Chem. Phys. Lett.* **1995**, *243*, 409.
[53] E. F. Kjønstad, R. H. Myhre, T. J. Martínez, H. Koch, *J. Chem. Phys* **2017**, *147*, 164105.
[54] S. Gozem, A. I. Krylov, M. Olivucci, *J. Chem. Theory Comput.* **2013**, *9*, 284.

[55] M. Huix-Rotllant, M. Filatov, S. Gozem, I. Schapiro, M. Olivucci, N. Ferré, *J. Chem. Theory Comput.* **2013**, *9*, 3917.
[56] S. Gozem, F. Melaccio, R. Lindh, A. I. Krylov, A. A. Granovsky, C. Angeli, M. Olivucci, *J. Chem. Theory Comput.* **2013**, *9*, 4495.
[57] R. Ditchfield, W. J. Hehre, J. A. Pople, *J. Chem. Phys.* **1971**, *54*, 724.
[58] B. Helmich-Paris, *J. Chem. Theory Comput.* **2019**, *15*, 4170.
[59] L. Wang, W. Xu, C. Yi, X. Wang, *J. Mol. Graphics Modell.* **2009**, *27*, 792.
[60] L. Vetráková, V. Ladányi, J. Al Anshori, P. Dvořák, J. Wirz, D. Heger, *Photochem. Photobiol. Sci.* **2017**, *16*, 1749.
[61] S. D. Folkestad, E. F. Kjønstad, R. H. Myhre, J. H. Andersen, A. Balbi, S. Coriani, T. Giovannini, L. Goletto, T. S. Haugland, A. Hutcheson, et al., *J. Chem. Phys.* **2020**, *152*, 184103.
[62] M. Schreiber, M. R. Silva-Junior, S. P. A. Sauer, W. Thiel, *J. Chem. Phys.* **2008**, *128*, 134110.
[63] A. C. Paul, R. H. Myhre, H. Koch, *J. Chem. Theory Comput.* **2021**, *17*, 117.
[64] M. R. Silva-Junior, S. P. Sauer, M. Schreiber, W. Thiel, *Mol. Phys.* **2010**, *108*, 453.
[65] S. D. Folkestad, E. F. Kjønstad, H. Koch, *J. Chem. Phys.* **2019**, *150*, 194112.
[66] E. Cancès, B. Mennucci, *J. Math. Chem.* **1998**, *23*, 309.
[67] T. Helgaker, P. Jørgensen, J. Olsen, *Molecular Electronic Structure Theory*, 1st ed., Vol. 0, Wiley, Chichester **2000**.
[68] S. Bai, R. Mansour, L. Stojanović, J. Toldo, M. Barbatti, *J. Mol. Model.* **2020**, *26*, 107.

SUPPORTING INFORMATION

Additional supporting information may be found online in the Supporting Information section at the end of this article.

How to cite this article: A. Hutcheson, A. C. Paul, R. H. Myhre, H. Koch, I.-M. Høyvik, *J Comput Chem* **2021**, *42*(20), 1419. https://doi.org/10.1002/jcc.26553